Motion of tethered instrumentation platforms for acoustic Doppler velocimetry in energetic tidal flows

Samuel Harding[a,*], Levi Kilcher[b], Jim Thomson[c]

[a] *Pacific Northwest National Laboratory, Richland, Washington, USA*
[b] *National Renewable Energy Laboratory, Golden, Colorado, USA*
[c] *Applied Physics Laboratory, University of Washington, Seattle, Washington, USA*

Abstract

The deployment of acoustic Doppler velocimeters (ADVs) on tethered instrumentation platforms has recently been investigated for the characterization of turbulence for the emerging tidal energy industry. A variety of instrumentation platforms have been deployed as part of this work including the streamlined StableMoor™ buoy (SMB), the Tidal Turbulence Mooring (TTM) system based on a conventional 0.9 m spherical buoy, and a 100 lb sounding weight. The first two systems are bottom mounted moorings and the latter is deployed from a research vessel. The motion-induced velocities at the ADV head on each platform type and instrument configuration are discussed in the context of flow energies relevant to tidal energy and with the objective of reducing motion contamination of measurements.

The SMB with a single ADV head mounted on the nose provided the most stable platform for the measurement of tidal turbulence in the inertial sub-range for flow speeds exceeding 1.0 ms^{-1}. The modification of the SMB with a transverse wing configuration for multiple ADVs showed a similar frequency response to the nose configuration but with large contamination in the vertical direction as a result of platform roll. While the TTM provided a relatively stable configuration at low frequencies of motion, the motion-induced velocity at the ADV head became significant at frequencies above $f > 1$ Hz. The sounding weight measurements showed the greatest motion at the ADV head but are likely to be influenced by both prop-wash and vessel motion.

*Corresponding author
Email address: samuel.harding@pnnl.gov (Samuel Harding)

Keywords: Tidal turbulence, Tethered platform, ADV, Tidal energy

1. Introduction

The kinetic energy of tidal currents presents a valuable source of renewable energy. For this application, the understanding of the flow behavior is critical to the design and operation of a tidal energy conversion device. The interest in understanding mid-water oceanic turbulence also extends to the fields of marine microbiology, ecology, mooring technologies, thermal mixing and chemical stratification. Though the mean kinetic energy and bulk turbulence statistics of a tidal site can be characterized with relative ease using acoustic Doppler current profilers (ADCPs), the higher temporal and spatial resolution required to detect the full range of turbulent scales in an energetic tidal site poses a greater measurement challenge.

Understanding the turbulence characteristics at the hub depth of the marine hydro-kinetic (MHK) device is of particular interest. This is the location where the flow is ultimately converted from kinetic energy to electricity, and so the fluctuating component of the flow is not only manifested in unsteady hydrodynamic loading conditions (McCann, 2007; Milne et al., 2010; Afgan et al., 2013), but also in the energy output.

A wide range of MHK concepts are currently in development, however many concepts reflect the common depth profiles which indicate that the peak available energy is found at mid-depths of the vertical velocity profile (Legrand, 2009). Locations close to the seabed exhibit lower flow speeds due to the flow shear created by friction forces. Hub heights approaching the free surface are susceptible to the unpredictable meteorologically-driven surface dynamics. It follows that the typical energy extraction location of an MHK device is difficult to physically access from either fixed bottom-mounted or vessel-mounted deployments prior to prototype installations.

Many key properties of tidal turbulence are able to be directly characterized by high frequency point velocity measurements. This is most widely achieved in the field through the use of an acoustic Doppler velocimeter (ADV), which uses a bi-static configuration of transmitters and receivers to measure a sample volume of approximately 1 cm^3 with high temporal resolution.

The challenge with deploying a point-measurement velocimeter is accessing the areas of interest in the water column. Large hydrodynamic loads and moments are generated on structures which are fixed to the ocean floor or penetrate from the surface. These moments can be mitigated through the use of compliant mooring lines to submerged instrumentation. With the removal of fixed structures under moored configurations, the motion of the instrument relative to the motion of the water can become significant (Thomson et al., 2013; Paskyabi and Fer, 2013; Matt et al., 2014).

Meaningful velocity measurements of tidal turbulence can be achieved through the measurement and removal of the platform motion from the measured velocity (Kilcher et al., 2014a; Thomson et al., 2013, 2014). In this process, the motion of submerged instrumentation platforms are measured using inertial measurement units (IMUs), to detect both the linear acceleration in the earth coordinate frame as well as the angular rotation rate in pitch, roll and yaw.

Persistent motion contamination is observed when the motion-induced velocity at the ADV head was large. The motion contamination can thus be minimized through the selection of the most stable platform for the velocity measurements. In short, 'the best form of motion correction is motion prevention' (Jim Thomson, pers. comm.). This paper presents the motion-induced velocity at the ADV head mounted on a range of sub-sea platform geometries and configurations which were deployed in work presented by Kilcher et al. (2015) in Part 1 of this paper. This approach is similar to that used in the motion-correction of shipboard atmospheric measurements, such as those presented by (Edson et al., 1998).

As an appendix to this work, the platform motion over a wide range of frequencies is calculated by combining the low frequency bottom tracking capabilities of an ADCP with the high frequency IMU measurements.

2. Instrumentation

2.1. Inertial measurement units

The IMU used in the following experiments is the LORD MicroStrain 3DM-GX3-25-OEM inertial sensor (LORD MicroStrain, 2014). This unit is a industrial grade attitude heading and reference system (AHRS) with integrated magnetometers, with a form factor of $38 \times 24 \times 12$ mm. The IMU was integrated into the Nortek Vector ADVs with tight time synchronization, with the unit axes orthogonal to the axes of the ADV body (pressure case).

The calculation of the ADV head motion from the IMU output is presented in Part 1 of this paper (Kilcher et al., 2015).

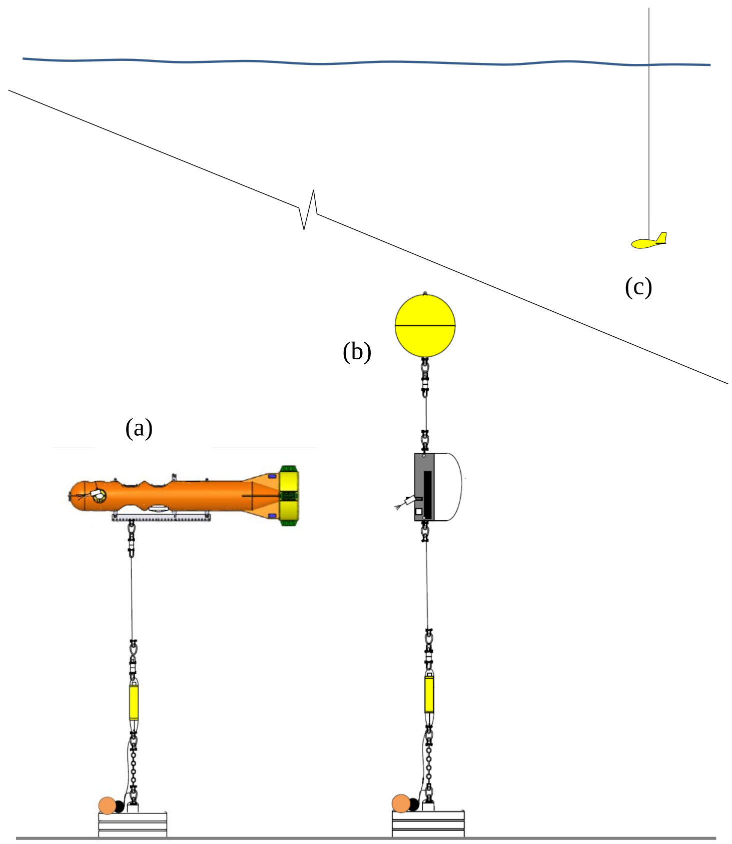

Figure 1: Platform schematics: (a) StableMoor™ buoy (SMB), (b) Tidal Turbulence Mooring system (TTM) and (c) sounding weight tethered to the research vessel.

2.2. Mooring hardware

Three instrumentation platforms for ADV deployments were considered in this motion comparison analysis. Each platform is introduced in the following subsections. A schematic of all three platforms is shown in Figure 1 with key parameters summarized in Table 1.

2.2.1. StableMoor™ buoy platform

The streamlined StableMoor™ mooring buoy (SMB) is an instrumentation platform produced by DeepWater Buoyancy, Inc. (formerly designed by Flotation Technologies). The buoy is manufactured using syntactic foam with a protective GRP shell. The elongated form of the buoy and GRP

Table 1: Velocimetry platform properties.

Platform	Fastening location	Streamwise platform length (m)	Line length, L (m)	Dry mass, m (kg)	Submerged mass[1] (kg)
SMB	Seabed	3.6	9.5	-	-180
TTM	Seabed	0.9	11	137	-300
Sounding weight	Vessel	0.4	20, 30, 40	45	41

[1] Negative values indicate net buoyancy

tail vane are designed to reduce drag loads and increase dynamic stability is energetic flow conditions.

In this study, ADVs were mounted to the SMB in two configurations, both with the ADV head in the upward looking direction:

- Winged-mode: A carbon-fiber beam with an elliptical cross-section was installed near the nose of the SMB with a port and starboard ADV attached to either end, as shown in Figure 2a. The ADV bodies where installed in the instrumentation wells in the SMB body.

- Nose-mode: The carbon-fiber beam was removed and a single ADV was installed, with the ADV head attachment protruding from the nose of the SMB, as shown in Figure 2b.

2.2.2. Tidal Turbulence Mooring platform

The Tidal Turbulence Mooring (TTM) system uses two ADVs are mounted to a vane which is then fixed to a mooring line between an anchor on the seabed and a 0.9 m spherical buoy. This is the same configuration as used in previous experiments by Thomson et al. (2013). The principal components of the TTM are shown in Figure 3.

2.2.3. Sounding weight platform

The sounding weight used in these experiments is a streamlined instrumentation platform is suspended below the research vessel. The 100 lb USGS 'Columbus-type' weight is cast from lead, with aluminum tail fins. A davit was used to deploy the sounding weight over the port side of the vessel as

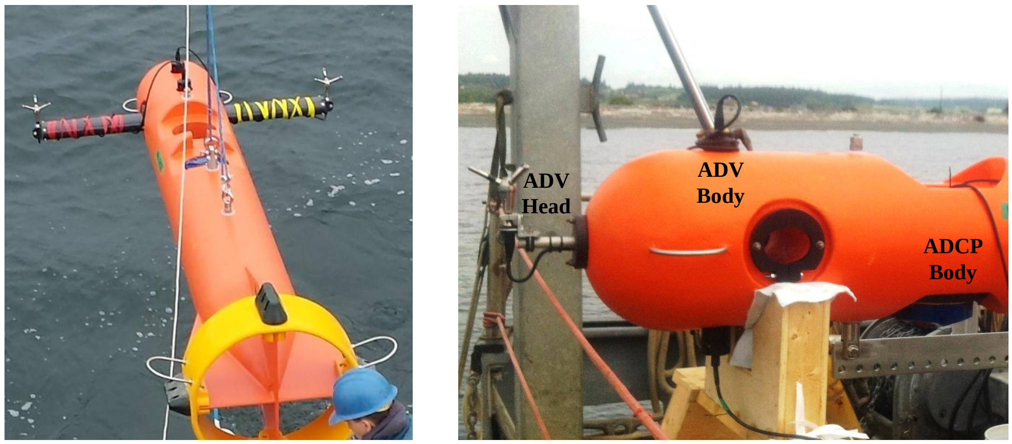

(a) (b)

Figure 2: StableMoor™mooring buoy configurations: a) Two ADVs in winged-mode and b) a single ADV in nose mode.

(a) (b) (c)

Figure 3: TTM components: a) Seabed anchor constructed using three railroad wheels, b) two ADVs on strong-back vane attached to mooring line and c) spherical buoy at end of mooring line.

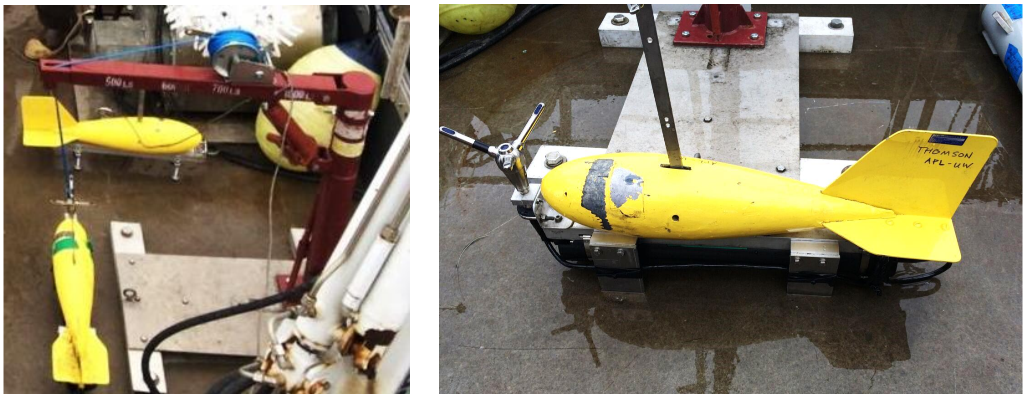

(a) (b)

Figure 4: Sounding weight platform: a) sounding weight tethered to davit for vessel mounted deployment and b) ADV head configuration.

shown in Figure 4a. The cabled ADV head was installed in an upwards looking orientation at the nose of the sounding weight, as shown in Figure 4b.

3. Coordinate System

The linear and angular motion of the each platform is measured by the IMU in the mounted ADV body and the motion correction is performed in the earth coordinate frame. All velocity signals are then rotated into a right-handed platform coordinate system such that $\vec{u}_m^{\,p}(t) = (v_1, v_2, v_3)$ where v_1 is aligned with the longitudinal axis of the platform (positive towards nose), v_2 is the transverse direction and v_3 is aligned in the vertical direction (positive up).

Performing the platform motion characterization in the principal coordinate system (aligned with the principal flow direction) caused cross contamination between the motion signal in the stream-wise and cross-flow directions at this site. This is due to the asymmetry in the ebb and flood flow direction at the deployment location (Polagye and Thomson, 2013). Some level of directional asymmetry is often observed in tidal flows, and for this reason the authors suggest the use of platform coordinates in such motion analysis.

The motion-induced velocity measured by the ADV, ($\vec{u}_m(t)$), is computed from the IMU rotation rate vector ($\vec{\omega}$) and the linear acceleration vector ($\overrightarrow{a}$) using Equation 1.

$$\overrightarrow{u}_m(t) = \overrightarrow{\omega}(t) \times \overrightarrow{l} + \int \overrightarrow{a}'(t)\mathrm{d}t \tag{1}$$

Here l is the vector from the IMU to the ADV sensor-head and $\overrightarrow{a}'$ is the high-pass filtered IMU acceleration. For more details on this process, refer to Part 1 of this paper by Kilcher et al.

4. Motion-induced velocity results

4.1. Frequency response

The motion-induced velocity measured by the ADV is presented in the frequency domain in the same way as TKE spectra are present for the flow in which they are deployed. Specifically, spectra are calculated using a fast Fourier transform ($\mathscr{F}$) of the motion-induced ADV velocity was calculated using 128 s of detrended, hanning-windowed segments with 50% overlap, such that $S\{u\}(f) = |\mathscr{F}(u)|^2$.

The frequency response amplitude, $H\{\overrightarrow{u}\}(f)$, relates the TKE spectra, $S\{\overrightarrow{u}\}(f)$, (presented in Part 1) to the energy spectra of the motion-induced velocity at the ADV head, $S\{\overrightarrow{u}_m\}(f)$, as defined in Equation 2. This method is analogous to the processing of the frequency response amplitude of a signal.

$$H\{\overrightarrow{u}^p\}(f) = \frac{S\{\overrightarrow{u}^p_m\}(f)}{S\{\overrightarrow{u}^p\}(f)} \tag{2}$$

The frequency response function in the direction of the longitudinal, transverse and vertical axis of the platform are denoted as $H\{v_1\}$,$H\{v_2\}$ and $H\{v_3\}$, respectively.

Persistent motion contamination was observed when the frequency response amplitude was large. At these frequencies the velocity correction process was not able to totally remove the motion-induced velocity at the ADV head, resulting in irregularities in $S\{\overrightarrow{u}^p\}(f)$. The velocity spectra were interpolated across the contaminated frequencies before calculation of the frequency response in Equation 2 to avoid the propagation of errors. For this reason the frequency response amplitude has been used in this analysis rather than the conventional transfer function definition[1] as the motion con-

[1] Defined as the ratio between the cross-power spectral density of the motion-induced velocity and the flow velocity, and the power spectral density of the velocity

tamination was not able to be removed from the cross power spectral density term.

4.1.1. StableMoor™ buoy

The motion-induced ADV energy spectra is presented in Figure 5 for all tested ADV configurations. This figure groups the velocity spectra in terms of the mean flow velocity, U, in increments of 0.5 ms^{-1}.

The motion-induced ADV velocity for the starboard and port instruments in winged mode (top and middle plots in Figure 5, respectively) demonstrated very similar motion characteristics, with the majority of the motion energy is found in the frequency range of 0.07-0.2 Hz. In general, the motion of the instrument increases at higher mean flow velocities. The frequency response amplitude is very similar between the two configurations in all directions for $f \leq 0.3$ Hz. In this low frequency range, the motion is predominantly in the lateral direction. The motion can be visualized as a 'swimming' dynamic where the platform yaws about the z-axis. The peak energy spectra of the motion-induced velocity at the ADV head, $S\{v_2\}(0.07\ \mathrm{Hz}) \approx 0.1\ \mathrm{m}^2\mathrm{s}^{-2}\mathrm{Hz}^{-1}$. The period of this motion is 14 s with an amplitude of approximately 0.7 m.

A natural frequency phenomena is observed at 0.8 Hz in the transverse and vertical directions at low flow speeds, with a maximum response in the $0.5 < U \leq 1.0\ \mathrm{ms}^{-1}$ velocity band. The frequency response was calculated for the mean velocity range where the high frequency resonance was observed, $0 < U \leq 1.0\ \mathrm{ms}^{-1}$. Figure 6 shows the key dynamics of the SMB motion for the winged configuration (port ADV) and nose configuration.

The higher frequency resonance is observed in the frequency response amplitude for the transverse motion and also observed in vertical direction in winged mode. As the SMB moves in the lateral direction, the mooring line fastened to the underside of the buoy causes a rolling motion at the same frequency. In the case of the winged configuration, the angular velocity of the roll is translated into a vertical motion of the ADV heads which are mounted on a horizontal moment arm. This introduces a strong rotation-induced vertical velocity at the same frequency as the lateral motion, at $f = 0.8$ Hz.

4.1.2. Tidal Turbulence Mooring

The motion-induced ADV velocity in the TTM configuration is a function of two dynamic phenomena. Firstly, the motion of the spherical buoy dominates the motion of the system at the natural frequency of the pendular

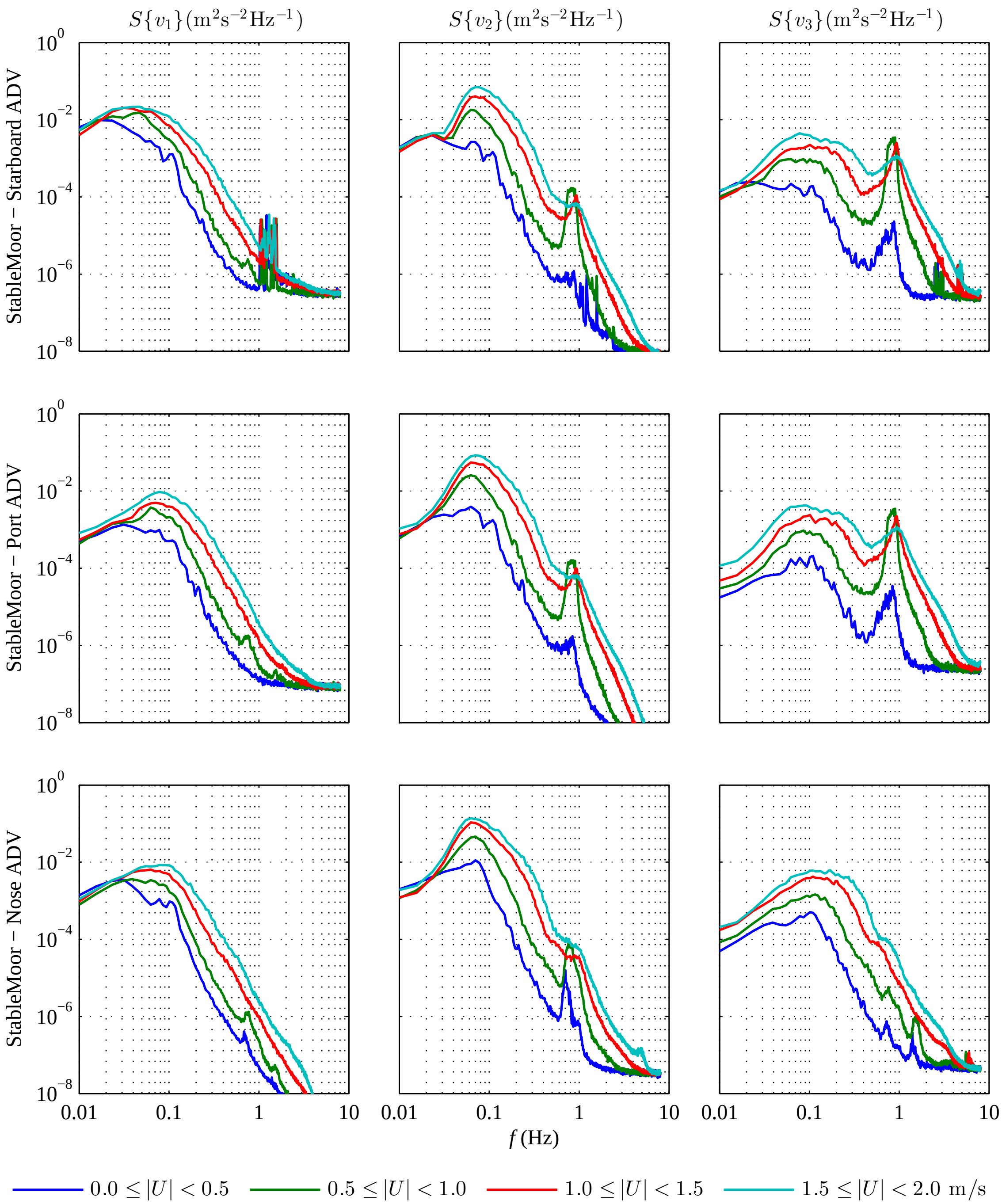

Figure 5: StableMoor motion for ADV deployments in winged mode (top and middle), and nose mode (bottom).

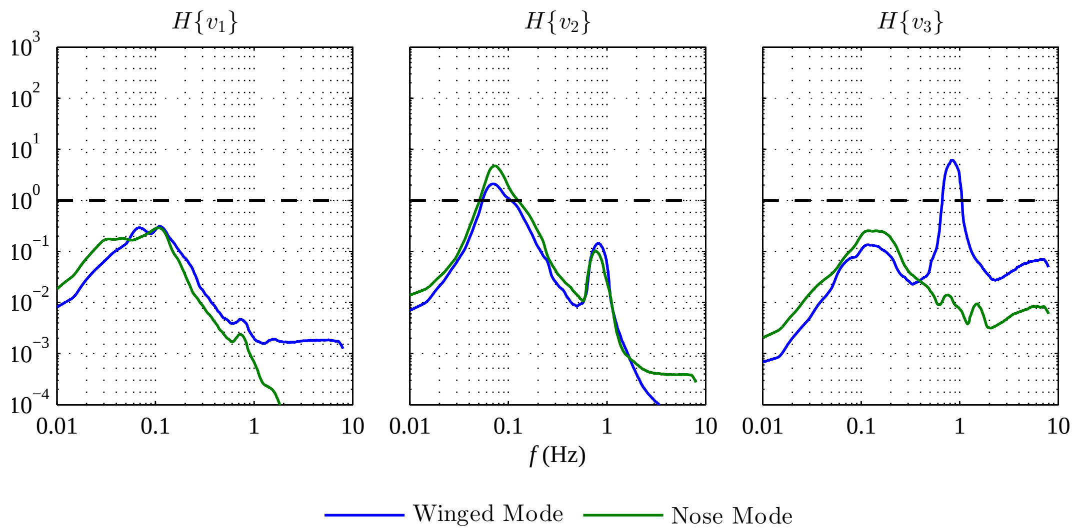

Figure 6: Frequency response amplitude of StableMoor ADV motion for velocity range $0 \leq U < 1$ ms^{-1} for starboard ADV in winged mode and nose ADV.

system. The ability of the ADV mounting board to yaw about the mooring line also introduces a lateral motion of the ADV head. The frequency response amplitude calculated for the motion of the TTM system is presented in Figure 7.

The dominant motion of the system, particularly at low flow speeds, results from the vortex induced velocity (VIV) of the large spherical mooring buoy at the end of the mooring line (Figure 3c). This configuration can be interpreted as a buoyant pendulum system, with a natural frequency described as a function of the Strouhal number of the spherical buoy, S_n, by Equation 3.

$$f_n = \frac{US_n}{D} \tag{3}$$

After verifying that the drag force may be neglected, the Strouhal number can be approximated to account for added mass by using Equation 4 (Williamson and Govardhan, 1997; Govardhan and Williamson, 2005). Here $Fr = U/\sqrt{gD}$, m^* is the sphere mass normalized by the displaced mass of fluid ($m^* = m/(\frac{1}{6}\pi D^3\rho)$), and C_A is the added mass coefficient equal to 0.5.

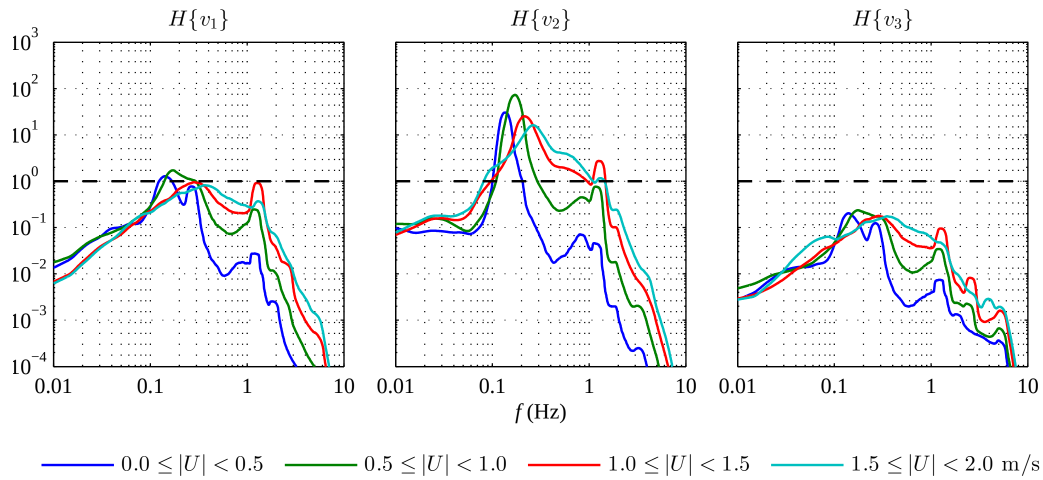

Figure 7: TTM frequency response amplitude

$$S_n \approx \frac{1}{2\pi Fr\sqrt{L/D}}\sqrt{\frac{1-m^*}{C_a+m^*}} \tag{4}$$

By substituting Equation 4 into Equation 3, the theoretical natural frequency of the buoyant spherical pendulum is calculated as 0.13 Hz. The peak motion frequencies measured in the lateral direction are in the range of $0.10 - 0.25$ Hz. The comparable frequencies of this motion is interpreted as confirmation of the *a priori* assumption of vortex-induced motion of the spherical buoy.

The higher frequency motion-induced ADV velocities measured in the lateral direction is attributed to the ability for the ADV vane to yaw about the mooring line in a fluttering motion. As such, the stream-wise and vertical motion at this frequency are significantly lower than the transverse motion. Evidence of motion in these directions at the same frequency is due to the mooring line deviating from vertical due to blow-down of the TTM system to an angle of 20° at mean flow speeds of 2.0 ms^{-1} (Thomson et al., 2013).

4.1.3. Sounding weight

The frequency response amplitudes of the motion-induced velocity of sounding weight ADV are presented in Figure 8. The sounding weight was deployed from the research vessel as it was holding station in flow speeds of $1.0 < U \leq 1.5$ ms^{-1}. The port deployments used the davit for deployment

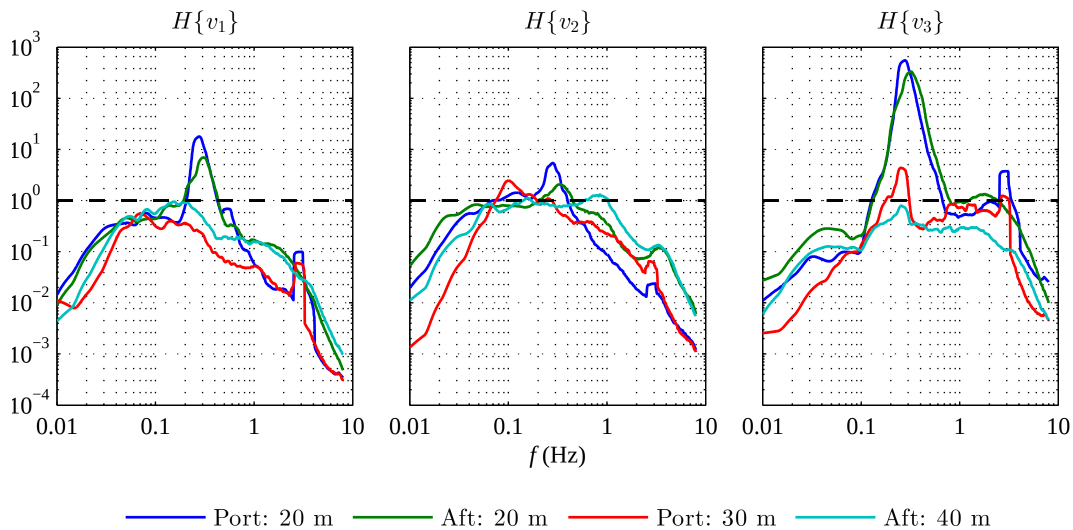

Figure 8: Comparison of sounding weight

with a thin line. The aft deployments utilized the A-frame winch, with a relatively thick tethering line.

The primary motion of the sounding weight is a pitching-heaving dynamic at a frequency of $f \approx 0.27$ Hz. The amplitude of this motion is significantly greater at the shorter line lengths of 20 m, and decreases as the line length is increased. The angle of the line was seen to increase with line length which may also be responsible for some change in motion dynamics. The port deployment shows greater motion than the aft, which may be due to the thicker tethering line providing increased motion damping in the latter.

Neglecting the effect of added mass and drag allows the deployed sounding weight to be modeled as a pendulum with the frequency of Equation 5, where T is equal to the tension in the line after accounting for buoyancy effects (Govardhan and Williamson, 1997).

$$f_n \approx \frac{1}{2\pi}\sqrt{\frac{T}{mL}} \tag{5}$$

Using Equation 5, the theoretical natural frequencies for the line lengths of 20, 30 and 40 m are 0.11, 0.09 and 0.08 Hz, respectively. Though the frequency response amplitude of the sounding weight motion does not show a very steep resonance peak, the approximation of the peak frequency given by Equation 5 is within the frequency range of maximum motion of $0.08 \leq f \leq 0.4$ Hz in the transverse direction.

The motion of the sounding weight is subject to forcing terms not found in the SMB and TTM. Firstly, the instrument is tethered to the research vessel which is holding station in the unsteady flows and affected by surface dynamics (waves and swell). This introduced an additional velocity source not found in the seabed tethered systems. As a result of this deployment method, the ADV may also be exposed to the prop-wash aft of the propellers, which is particularly significant for the shorter tethering lines and instrument deployed from the aft rather than the port. The deployment of each sounding weight was limited to between $30 - 60$ minutes so the frequency response of Figure 8 represents significantly less data than the SMB and TTM deployments. While strumming was observed in the lines above the water level, the frequency of this exceeds that captured by the ADV-IMU and the resulting motion-induced velocity at the ADV head is expected to be negligible. The combination of these factors make direct comparison of the sounding weight with the SMB and TTM deployments difficult.

5. Platform motion comparison

The ADV motion of a range of platform configurations discussed herein is presented in Figure 9. These spectra represent the motion-induced velocities at the ADV head for flow conditions in the range of $1.0 \leq U < 2.0$ ms^{-1} as the velocity range most relevant to the application of tidal energy.

In the stream-wise direction the SMB platform is significantly more stable than the TTM at $f > 0.1$ Hz, with an order of magnitude reduction in motion induced velocities for $f > 1.0$ Hz. This high frequency stability is comparable in the transverse direction. Though there is evidence of the SMB natural frequency at $f \approx 0.8$ Hz the motion-induced velocities remain significantly lower than the TTM platform. This is particularly significant in the context of turbulence measurements which utilize the higher frequency capabilities of the ADV to characterize the inertial sub-range.

The TTM is at least as stable as the SMB and sounding weight at lower frequencies ($f < 0.1$ Hz) in all directions. However at frequencies above the threshold, the motion induced velocity of the TTM ADV in the stream-wise and lateral directions is the greatest of all the platform configurations shown. In particular, the VIV frequency of the spherical buoy causes a peak in the motion of the TTM at $f \approx 0.13$ Hz.

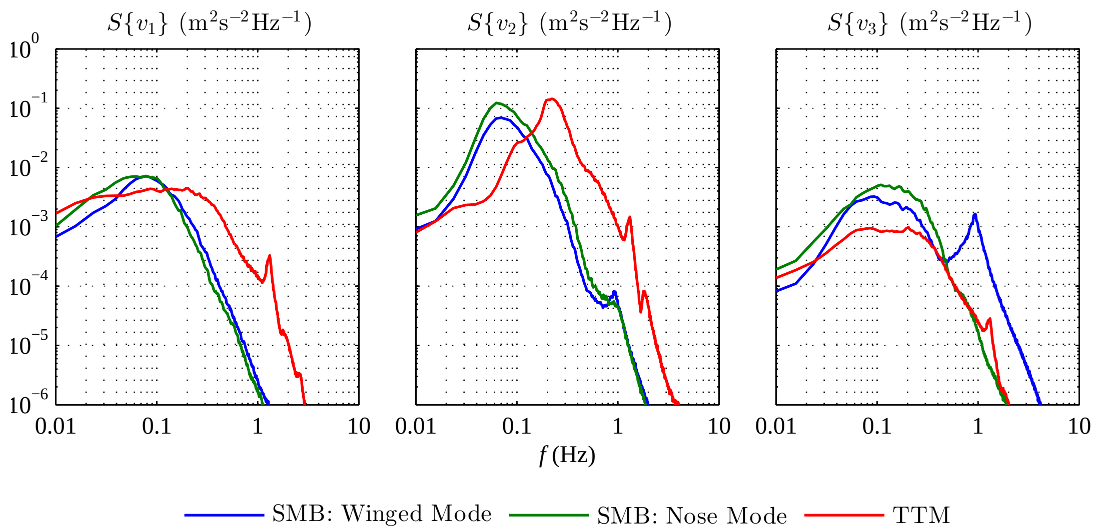

Figure 9: Motion-induced ADV velocity spectra for range of instrumentation platforms and configurations.

However, the TTM is the most stable platform at all frequencies in the vertical direction. This is particularly important in the use of ADVs to characterize turbulence, because the vertical component of velocity is the cleanest measurement from the ADV head in the configurations deployed as a result of the beam geometry. As a result, for isotropic turbulence, this velocity component provides the best estimate of TKE dissipation rate via the inertial sub-range. The TTM is therefore the most appropriate mooring for this use, though its performance is inferior in the other directions of motion.

6. Conclusions

Tethered instrumentation platforms are able to be used to deploy ADVs in energetic tidal environments through the development of motion correction calculations introduced in Part 1 of this paper. However, large motion-induced velocities at the ADV head can result in persistent motion contamination of the corrected velocity signal. The platform motions analyzed show that the frequency response is sensitive to the flow speed and the platform geometries and configurations.

To summarize, the SMB with a single ADV deployed on the nose provided the most stable ADV measurement, with superior frequency response at $f > 0.1$ Hz. This resulted in an uncontaminated motion-corrected measurement of the velocity spectra throughout the inertial sub-range of the turbulence measurement. When the SMB was deployed in wing mode, the roll of the platform induced a significant vertical velocity component at the ADV-head at $f \approx 0.8$ Hz. While providing a stable platform at relatively low frequencies ($f < 0.1$ Hz) and in the vertical direction, the motion at the TTM ADV was an order of magnitude larger than that of the SMB in the stream-wise and transverse directions for most of the frequencies corresponding to the inertial sub-range turbulence at the deployment site.

The performance of the sounding weight platform showed a very large oscillatory component in the vertical direction for the 20 m deployments as the platform became unsteady in pitch. For the case of the sounding weight, the induced motion is a function of both the platform dynamics and the vessel motion to which it is coupled. The resulting motion contamination is the largest for all the platforms considered in these tests over most of the frequency range considered.

7. Acknowledgments

The authors would like to thank Joe Talbert and Alex de Klerk for the fabrication and preparation of the moorings as well as engineering support during the field operations. The authors thank Capt. Andy Reay-Ellers for his assistance in the precise deployment and retrieval of mooring hardware.

References

Afgan, I., McNaughton, J., Rolfo, S., Apsley, D. D., Stallard, T., Stansby, P., 2013. Turbulent flow and loading on a tidal stream turbine by LES and RANS. International Journal of Heat and Fluid Flow 43, 96–108.

Edson, J. B., Hinton, A. A., Prada, K. E., Hare, J. E., Fairall, C. W., 1998. Direct Covariance Flux Estimates from Mobile Platforms at Sea. Journal of Atmospheric and Oceanic Technology 15 (1991), 547–562.

Govardhan, R., Williamson, C., 1997. Vortex-induced motions of a tethered sphere. Journal of Wind Engineering and Industrial Aerodynamics 69-71, 375–385.

Govardhan, R. N., Williamson, C. H. K., 2005. Vortex-induced vibrations of a sphere. Journal of Fluid Mechanics 531, 11–47.

Kilcher, L., Thomson, J., Colby, J., 2014a. Determining the spatial coherence of turbulence at MHK sites. In: 2nd Marine Energy Technology Symposium. Seattle, WA.

Kilcher, L., Thomson, J., Talbert, J., Deklerk, A., 2014b. Measuring turbulence from moored acoustic Doppler velocimeters: A manual to quantifying inflow at tidal energy sites. Tech. rep.

Legrand, C., 2009. Assessment of Tidal Energy Resource. Tech. rep., European Marine Energy Centre Ltd.

LORD MicroStrain, 2014. LORD Datasheet: 3DM-GX3-25-OEM, OEM Attitude Heading Reference System (AHRS).

Matt, S., Hou, W., Woods, S., Goode, W., Jarosz, E., Weidemann, A., 2014. A novel platform to study the effect of small-scale turbulent density fluctuations on underwater imaging in the ocean. Methods in Oceanography 11 (2014), 39–58.

McCann, G., 2007. Tidal current turbine fatigue loading sensitivity to waves and turbulence a parametric study. In: 7th European Wave and Tidal Energy Conference. Porto, Portugal.

Milne, I., Sharma, R., Flay, R., Bickerton, S., 2010. The Role of Onset Turbulence on Tidal Turbine Blade Loads. In: 17th Australasian Fluid Mechanics Conference.

Paskyabi, M. B., Fer, I., 2013. Turbulence measurements in shallow water from a subsurface moored moving platform. Energy Procedia 35 (January), 307–316.

Polagye, B., Thomson, J., 2013. Tidal energy resource characterization: methodology and field study in Admiralty Inlet, Puget Sound, WA (USA). Proceedings of the Institution of Mechanical Engineers, Part A: Journal of Power and Energy 227 (3), 352–367.

Thomson, J., Kilcher, L., Richmond, M., Talbert, J., DeKlerk, A., Polagye, B., Guerra, M., Cienfuegos, R., 2013. Tidal turbulence spectra from a compliant mooring. In: 1st Marine Energy Technology Symposium (METS2013). Washington, D.C.

Thomson, J., Kilcher, L. F., Harding, S., 2014. Multi-scale coherent turbulence at tidal energy sites. In: 5th International Conference on Ocean Energy (ICOE2014). Halifax, Nova Scotia, pp. 1–6.

Williamson, C. H. K., Govardhan, R., 1997. Dynamics and Forcing of a Tethered Sphere in a Fluid Flow. Journal of Fluids and Structures 11, 293–305.

Appendix A. Combined motion spectra of ADV-IMU and ADCP-BT

Appendix A.1. Introduction

The motion of a tethered instrumentation platform was recorded using two methods of measurement; an inertial measurement unit (IMU) integrated with an acoustic Doppler velocimeter (ADV), and the bottom-tracking (BT) functionality of an acoustic Doppler current profiler (ADCP). The IMU motion is recorded at relatively high frequency but is unable to capture low frequency linear velocities due to the inherent signal drift of the integral of the measured acceleration. Conversely, the ADCP-BT is unable to capture high frequency motions (above the order of $f = 1$ Hz) due to the limitations in ping frequencies of the profiling instrument. This appendix outlines the process of combining the high frequency ADV-IMU motions with the low frequency ADCP-BT to calculate the motion-induced velocity spectra at the location of the ADCP, over a wide range of frequencies. An IMU-equipped ADV, and BT-capable ADCP were deployed on the tethered StableMoor instrumentation platform in Admiralty Inlet, WA for 24 hours from 12:00 on the 12th May 2015. The locations of the ADV and ADCP on the StableMoor platform are shown in Figure 2.

Bench-tests of the Microstrain IMU indicate that its accelerometers drift for frequencies less than 0.01 Hz. Therefore, in order to remove bias-drifts which cause large errors in $\overrightarrow{u}_a$, the measured $\overrightarrow{a}'(t)$ has been high-pass filtered with a threshold of $f_a = 0.033$ Hz (30 seconds) (Kilcher et al., 2014b). As a result, real motions at and below f_a will be underestimated using the ADV-IMU method.

The bottom-tracking method of the ADCP calculates the platform motion using the Doppler shift of acoustic pulses reflected from the seabed. The sample frequency of this method is limited to the order of $f = 1$ Hz, to avoid signal contamination due to ringing in the transducer head. The BT measurements are compensated for rotation-induced motion using the orientation sensors of the instrument. As such, the BT measurement represents the low frequency motion of the SMB at the ADCP location.

In this way, both the ADV-IMU and ADCP-BT can independently detect the motion of the tethered platform at the location of the ADCP within a limited frequency range, as shown for the transverse direction in Figure A.10. This plot shows some agreement between the two methods of measurement within the frequency band of $0.1 < f < 0.3$ Hz.

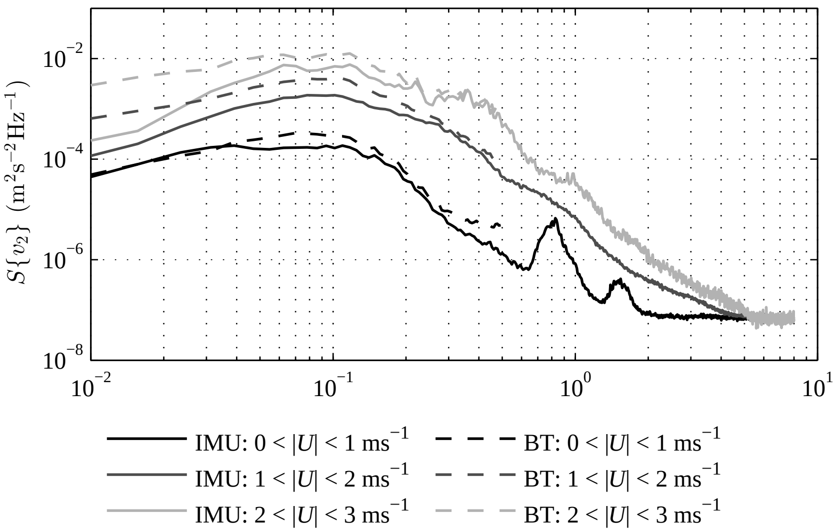

Figure A.10: Spectra of vertical ADCP motion in platform coordinate systems, using ADV-IMU and ADCP-BT methods for a number of mean flow velocities.

This appendix describes how the output of these instruments can be combined to calculate the motion of the platform, at the location of the ADCP, over a wider range of frequencies that using the ADV-IMU alone.

Appendix A.2. Methods

The following subsections outline the process of combining the ADV-IMU and ADCP-BT data sets to calculate the full spectra of platform motion. The following analysis is performed with all velocities in the platform coordinate system.

Appendix A.2.1. Clock synchronization

Accurate clock synchronization is required in order to combine the motion signals of the two instruments. Though both instruments were synchronized with GPS time during the week of deployment, clock drift was observed on the order of two seconds per day. Using the ADV clock as the reference time signal, the time difference of the ADCP was calculated using the cross-correlation of the vertical velocity time series, $z(t)$, using the following steps.

- Interpolate the BT velocity time series from the sample frequency of 1 Hz to the IMU frequency of 16 Hz.

- Divide the time series of both the IMU and BT derived motion into 120 s sub-series and calculate the time difference associated with the peak cross-correlation of each 120 s sub-series.

- Filter the spurious clock differences calculated at the slack tides, where the motion signal and resulting correlation was insufficient to detect significant cross-correlation.

- Fit a linear trend line to the clock difference as a function of time and calculate the offset and gain of the ADCP clock, relative to the ADV.

- Adjust the raw clock signal of the ADCP time series using the linear regression coefficients.

The ADCP clock began with an offset of 2.8 s, and drifted by 0.07 s per hour relative to the ADV clock.

Appendix A.2.2. Frequency response filter

Before the motion signals of the ADV-IMU and ADCP-BT methods can be combined, the signals must be attenuating using complementary filters such that the sum of the filter amplitudes is unity at all frequencies.

This achieved by using filter transfer functions which are symmetrical about the threshold frequency. The filter used in this analysis is a first-order Butterworth filter. The low-pass Butterworth filter is applied to the ADCP-BT motion, and the high-pass equivalent is applied to the the ADV-IMU motion.

Note that this high-pass filter has already been applied to the linear motion (not rotation-induced) component of the ADV-IMU motion in the *dolfyn* toolbox. Therefore, it is only applied to the rotation-induced component at this stage.

Appendix A.3. Results

The rotated motion vectors of each instrument were confirmed to have the same sign in the platform coordinate system. As such, the synchronized and filtered time-series of the platform motion were summed in the time domain. The spectra of the filtered motions from each instrument and the resulting combined motion signal is shown in Figure A.11.

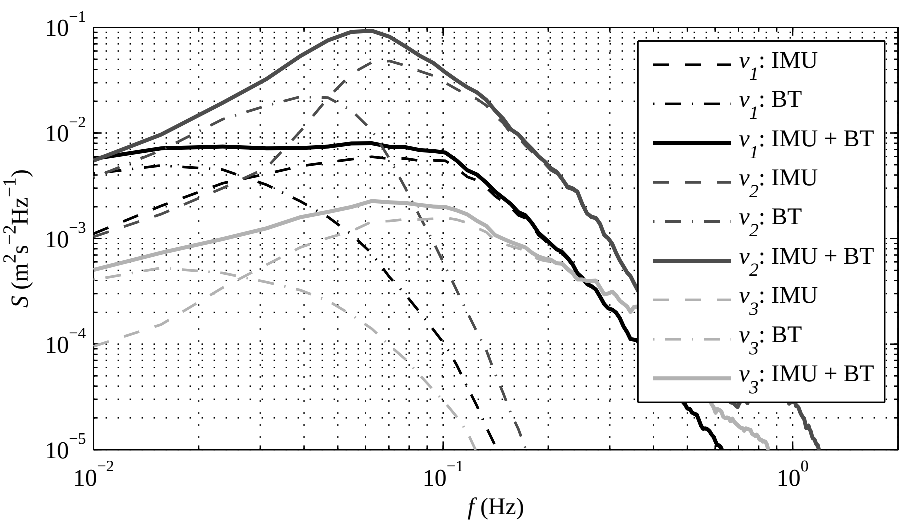

Figure A.11: Spectra of the combined filtered motion signals